HIGH PRODUCTIVITY VACUUM BLASTING SYSTEM

William S. McPhee (wsmcphee@home.com; (703) 566-0942)
LTC Teletrak, Inc., An Advanced Environmental Systems Company
P.O. Box 25432, Alexandria, VA 22313, USA
Fax: (703) 566-0972

C.X. Lin (Lin@eng.fiu.edu; (305) 348-1596)
B. Zheng, H.J. Kang, R. Ade, E. Shea, and M. A. Ebadian
Florida International University
Hemispheric Center for Environmental Technology
10555 West Flagler Street, Suite 2100
Miami, FL 33174, USA
Fax: (305) 348-1697

ABSTRACT

In order to increase the productivity and economics of an existing (or baseline) vacuum blasting technology, which has been used to remove radioactive contamination, PCBs, and lead-based paint at Department of Energy (DOE) sites, the redevelopment and design of certain components has been initiated. These new components include a new rectangular blast nozzle, a blasthead with a wind curtain and sensors, and a new dust separator. These have been designed and fabricated based on numerical estimated data derived by the development mathematical models. The mathematical models were validated by the experimental data with a deviation within ±10%. The results of pre-prototype testing indicated that the efficiency and economics of the redesigned blasting vacuum system with implementation of the above innovative components can be increased almost 50% over that of the baseline technology.

INTRODUCTION

Vacuum blasting has been used as an efficient technology for the decontamination of both large concrete and steel surface areas. This technology minimizes waste and provides worker protection by continuously recycling the blasting material and containing the dust during the decontamination process. However, to date, since the physical mechanism of two-phases flow in the complex configuration was not understood well, the current vacuum blasting technology still has limitations that can be improved.

Recent research, both from the open blasting industry and vacuum blasting done by Seavery (1985), McPhee and van Leeuwen (1988), Settles and Garg (1994), and from Settles and Gepprt (1996), McPhee, W.S., and Waagbo, S. (1992), and McPhee and Ebadian (1999 and 2000), indicates that there are three key components, including the blast nozzle, dust separators, and blasthead, which can affect the overall efficiency of the system significantly. Among these three, the redesign of the nozzle alone offers an estimated 80% increase in efficiency. Fine steel abrasives are important in improving the cleaning production rate, but such fine particles cannot

be efficiently separated from the dust using the existing separators. In a process based on the recycling of the abrasive, for the minimization of waste generation, this lack of efficiency of separation decreases that of the whole system. To reduce or even eliminate the operator dependency, the new blasthead will also need to incorporate sensors. These sensors will have two functions: 1) to trigger shut-down if the blasthead is taken from the surface; 2) to ensure neither "under or over" cleaning of a given surface area by providing highly desirable real-time characterization that determines the effectiveness of decontamination. Although much previous research has been done to increase the efficiency of the whole blasting system, there is almost no open literature about the systematic investigations on increasing the efficiency of the vacuum blasting system based on the three areas outlined above.

The present work focuses on redesigning and improving existing vacuum blasting technology by implementing some innovative components, including blasting nozzle, dust separators, and blasthead incorporated with sensors. The redesign is expected to enhance the productivity and economy of the vacuum blasting system by at least 50% over current vacuum blasting systems. The project includes numerical analysis, production of a prototype to test in a lab environment, and ultimate integration with LTC's Sealed Waste Transfer System (SWATSTM) and LTC's Vacuum Blasting machines.

The mathematical model was developed to simulate the entire process numerically. The verification test has been performed to validate the developed model and related code. The experimental results agreed with the numerical estimated data with a deviation within ±10%, thus proving the mathematical model and the model test successful. Based on the numerical prediction, the innovative components mentioned above have been designed, fabricated, and tested. The final testing of the pre-prototype under controlled conditions indicated that the productivity rate and economy of the redesigned system were increased almost 50% over the baseline technology. This is to be followed by the design and fabrication of the full commercial High Productivity Vacuum Blasting System. This full-scale prototype will then be tested at a DOE designated facility as to the system performance, the productivity, and the economy of the improved vacuum blasting system.

PART I. DEVELOPING AND TESTING MATHEMATICAL MODELS

Mathematical model of two-phase flow for blasting system

The two-phase (air-particle) model, incorporating some existing models, has been developed for simulating two-phase flow in the entire vacuum blasting system. The calculations were performed for the blasting nozzle, separator, and blasthead/wind curtain. In this numerical model, the air was treated as the continuous phase, and the particle was treated as the second discrete phase. The fully three- or two-dimensional Navier-Stokes equations were used to simulate the air flow in the certain components; for example, three-dimensional equations are used for nozzles and centrifugal separators, two-dimensional equations are used for wind curtain and vertical duct separator. The standard κ~ε model proposed by Launder and Spalding (1972) was used to model the turbulent flow in these components. The trajectory of the discrete phase particle was predicted by integrating the force balance on the particle, which was written in a Lagrangian reference frame. This force balance equated the particle inertia with the forces acting on the particle. The

dispersion of particles due to turbulence in the fluid phase is modeled using the stochastic discrete-particle approach (Fluent 1998; Morsi and Alexander 1972).

There are two sets of boundary conditions. The first one is for the continuous phase (air); the second is for the discrete phase (particle). For the continuous phase (air), a non-slip boundary condition was imposed on the wall. The total pressure, temperature, and static pressure were known at the nozzle entrance. At the nozzle exit plane, all flow quantities were extrapolated from the two neighboring interior planes upstream of the exit plane. For separator and blasthead/wind curtain, the uniform velocity profile was imposed in the inlet plane, and the fixed pressure was imposed in the outlet plane.

For the discrete phase (particle), the "escape" boundary condition was imposed in the inlet and the outlet planes. "Escape" means the particle will vanish when it encounters the boundary in question, then trajectory calculations will be terminated. The "reflect" boundary condition was imposed in the wall. "reflect" indicates the rebound of the particle from the boundary in question with a change in its momentum being defined by the coefficient of restitution. In this paper, the coefficient of restitution equal to 1.0 implied that the particle retained all of its normal momentum after the rebound (an elastic collision).

The upcouple approach was adopted in the present study due to the assumption that the continuous phase is not impacted by the presence of the discrete phase. Therefore, after the flow field is converged, the particle trajectories are computed based on a fixed continuous-phase flow field. The discrete phase was introduced by computing the particle trajectories for each discrete phase injection. The turbulent flow and particle trajectories in the above components were solved by the CFD solver, FLUENT 5 (Fluent 1998), which used a control-volume finite element method (CVFEM) similar to that introduced by Baliga and Patankar (1983) to solve the governing equations. Two kinds of standard steel grits were adapted in this study: G40 with a particle size of 820 μm and G80 with a particle size of 300 μm. Both have the specific gravity of 7.0 g/cm3.

Description of experimental setup and instrument for the model test

Figure 1 illustrates the experimental setup of flow velocity and separation efficiency measurement. The LTC Vacuum Blasting Machine has been used to produce the blasting air-particle two-phase flow, and the vacuum pipeline will be used to recycle the steel grit. As shown in Fig. 1, the air compressor generates the high-pressure air. The high-pressure air is divided into three pipelines. Pipeline 1 is connected to the vacuum generator to produce vacuum. Pipeline 2 is connected to the pressure vessel. The air flow from pipeline 2 controls the valves (inside the pressure vessel) so that the steel grit can be drained from the upper chamber to the lower chamber in the pressure vessel. Of the three pipelines, pipeline 3 is the most important one. This pipeline produces the air-particle two-phase flow when the air is mixed with the steel grit that is drained from the lower chamber of the pressure vessel. The air flow rate and the temperature are measured before the air is mixed with the grits.

The air-particle two-phase mixture flows through the blasting nozzle. At the exit of the nozzle, the steel grit particles have a higher velocity. Between the blasting nozzle and the collection box, there is a rectangular glass channel (305x305 mm2 (1x1 ft2))with a length of 610mm (2 ft), through which the steel particles pass as a high-speed jet (Fig. 2). The collection box collects the steel grit from the nozzle and is connected to the vacuum pipeline 4 used to recycle the grit, after transporting the grit particles in the machine (see Fig. 1).

Three instruments are installed to measure the air flow rate, air temperature, and air pressure. The Phantom v3.0 High Speed Digetor Motion Analysis System is used to measure the steel grit velocity and the steel grit concentration in the experimental setup. The complete Phantom system includes three major components: a high-speed camera, pulsed laser source, and PIV software. This system is the combination of a high-speed imager, capturing several thousand images per second, with the short duration sheet lighting formed by pulsed laser, which allows the creation of sharp, clear pictures of a cross-sectional area of the flow, as shown in Fig. 2.

The dust samples (a mixture of steel particle and dust) from the dust collection box were analyzed using a Phillips XL30 Scanning Electron Microscope. All images were collected without any preparation or coating. The beam accelerating voltage was 10.0 kV; the beam spot size was 4.0; and the detector was secondary electron. The images were printed to a videographic printer, Model UP-890MD from Sony, and to a Polaroid camera. A low magnification image was generated to present an overall picture of the particle. From the picture, the ratio of recycled steel particles with diameters of 300 μm or greater can be obtained.

Comparison of numerical results with experimental data

Blasting nozzle

The calculations were performed with the fully three-dimensional numerical model for both the existing round nozzle and the new rectangular nozzle. The particle velocity and concentration distribution at the exit plane were obtained, as shown in Fig. 3. The numerical results indicated that there were two major disadvantages that greatly limit the blasthead cleaning rate in the existing round nozzle. One is that the statistical average particle velocities on the exit plane of the nozzle were low, probably because the nozzle is too short to provide enough residence time for the steel grit in the nozzle. Another is that the particle distribution at the exit plane of the round nozzle was too concentrated, which results in a narrow particle path. Although the blasthead cleaning rate can be increased by increasing the length of the existing round nozzle, theoretically there still exist other substantial disadvantages in the configuration of the round nozzle.

The new rectangular nozzle was proposed to surmount the disadvantages of the existing round nozzle. Numerical investigations have been performed to choose the optimum parameter for the rectangular nozzle. Based on the above numerical results and from a practical application point of view, the optimal geometric parameters of the rectangular nozzle were determined. The rectangular nozzles with 6.4 mm (¼ inch) and 9.5mm (3/8 inch) hydrodynamic throat diameter were chosen as the reference for experimental designing. And their geometry and detail dimensions were determined based on numerical results. Under the same conditions, the particle velocity at the exit plane of the newly designed rectangular nozzle can be increased almost 50% more than that of the existing round nozzle, and the particle distribution on the exit plane is more reasonable, as shown in Fig. 3.

Table 1 provides a comparison of the measurements with the numerical results at the same conditions, and the magnitude of velocity is a statistical average magnitude. As shown in Table 1, the deviation of the experimental results from the modeling data is within ±10%. Therefore, the model chosen for the numerical simulation was correct. Also, both experimental and numerical data show that the particle velocity at the exit plane of the rectangular nozzle was increased by more than 50% ofthat of the existing round nozzle under the same conditions.

Table 1.
Comparison of the measurement results with numerical modeling data

Nozzle	Pressure	Velocity, m/s (measurements)	Velocity, m/s (numerical data)	Deviation
Circular nozzle	4.5 bar(65 psi)	48.8	54	10.0%
Circular nozzle	5.7 bar(83 psi)	58.3	64	9.8%
Rectangular	4.5 bar(65 psi)	82.1	91	9.9%
Rectangular	5.7 bar(82 psi)	112.0	101	10.0%

Dust separators

In order to determine the performance of the existing separator, numerical simulations have been carried out. Numerical results showed that the air flow is concentrated in the center of the cylinders. It is estimated that the relative concentrated air flow may bring some particles out of the separator during the separating process. The calculated results of the separation efficiency verifies the above conclusion.

The geometry and grid system of the new centrifugal separator is shown in Fig. 4, and almost 100,000 cells are used to discretize the computation domain. As also shown in Fig. 4, the particles with initial velocity enter the inlet (left side) of the centrifugal separator. The trajectory of these particles in a turbulent flow field on the whole separator can be obtained by the Discrete Random Walk (DRW) model. As for whole particles, due to the fluctuation function of the turbulent flow field of the continuous phase, some of them can escape from the outlet, while others will draw down to the bottom of the separator. The separation efficiency is defined as the ratio of the total particles escaped from the outlet divided with the total particles fed into the separators. The number of the total particles escaped from the outlet was obtained from the statistical average value for 10 computations. The calculated separation efficiency is about 70% for steel grit G80. Compared with the existing separator, the separator efficiency for steel grit G80 was almost double. Therefore, the new centrifugal separator can separate the finer grit well, and, of course, it can separate the coarse grit.

The model test for measuring the separation efficiency of the dust separator was performed to verify the mathematical model. For concrete wall surface, the separation efficiency of the centrifugal separator can reach 84.1% at the experimental condition. But the efficiency of the existing separator for this condition was 25% under the same condition. For coating on steel plate surface, the efficiency of the centrifugal separator can reach 73.5%. The efficiency of the existing separator for this condition was 30%. The above results prove the almost doubled efficiency and the improved separation efficiency to perfect status.

Table 2 lists the numerical and experimental results. Comparing the experimental separation efficiency result of this centrifugal separator with numerical data, the difference between numerical and experimental results is below ±10% (75% from numerical modeling data for this case; 84.1% and 73.5% from experimental results mentioned above). Table 2 lists all the comparison results. The experimental data and numerical modeling results agree very well; therefore, the design of the new centrifugal separator was successful.

Table 2.
Comparison of the measurement results with numerical modeling data

	Efficiency (numerical modeling)	**Efficiency (test data)**	**Deviation**
Existing separator	27%	25% (for concrete surface)	5%
		20% (for coating on steel plate surface)	10%
Newly designed centrifugal separator	75%	84.1% (for concrete wall surface)	10%
		73.5% (for coating on steel plate surface)	5%

In order to verify the modeling results, two different positions were chosen in order to obtain the centrifugal separator's internal velocity distribution. Two 12.7-mm (½ inch) holes were drilled on the external surface of the separator to measure the velocity distribution in the separator. One is 50.8 mm (2 inches) and the other is 152.4 mm (6 inches) from the separator's top surface. The two holes are on the opposite-side surface of the separator's tangential air-inlet channel. Two direction velocities (tangential direction along the cylinder surface and axial along the vertical direction) were measured to compare with the numerical simulation results. A 6060P Pitot probe from ALNOR INSTRUMENT COMPANY was employed to obtain the velocity distribution.

Figure 5 shows the results from experiment and numerical modeling of the lower hole. The direction of coordinates begins from the centerline of the separator to the air-inlet channel surface. Judging from these figures, the distinction of the experimental results and the estimated data agree fairly well with a deviation within ±10%. Therefore, it can be assumed that the numerical model and the newly designed separator are successful.

Numerical prediction of the wind curtain

The wind curtain is expected to have two functions. One is to create an air barrier to prevent the particles escaping into the atmosphere. The other is to make the blasthead float on the wall surface and balance the forces. To meet the above need, the configuration shown in Fig. 6 was adopted.

Because the wall surface can not be very smooth, a gap between the wall surface and the blasthead was considered. The injected air has a fixed pressure, and the geometry has an inclined angle. The numerical modeling was performed to study the air flow field for the wind curtain. For the air injection system, the channel gap and the channel inclined angle are the main parameters. The blasthead working distance is also an important parameter.

Three channel gaps of the wind curtain, of 1mm, 1.6mm (1/16 inch), and 3.2mm (1/8 inch), were chosen for numerical modeling. The numerical modeling was conducted for each channel gap with 30°, 45°, and 60° inclination angles. The assumed working distances are from 2.5mm (0.1 inch) to 76.2 mm (3 inch). The assumed working distance effects on wind curtain efficiency, which means the statistical percentage of particles contained inside the wind curtain, are dependent on the injection pressure. The numerical predictions showed that with an increase of the injection pressure, the wind curtain efficiency can be increased to near 100% under ideal conditions.

The lift force can also be balanced. The criteria of the optimum parameters are based on calculated results and a practical view. Under the conditions that the injection pressure is below 1.5 bar, the vacuum pressure is above 0.2 bar, and more than 95% of G80 grit will be contained inside the wind curtain, the following optimal parameters were proposed: the channel gap is 1mm to 2 mm; the inline angle is 45° to 60°; the working distance is 0~25.4mm (1 inch).

PART II. PROTOYPE DESIGN, FABRICATION, AND TESTING

Blasting nozzles

The new blast nozzle with a 6.4-mm (¼-inch) hydrodynamic throat diameter was designed based on numerical results, as shown in Fig. 7. To determine the optimum material for fabricating the nozzle liner, tungsten carbide, boron carbide, and Roctec 500 were selected for the fabrication of this component. "Lifetime" testing of the nozzle will also be performed in making a final selection.

Blasthead

The new blasthead, made of aluminum alloy, is shown in Fig. 8. The wind curtain will be formed with injection compressed air through three hollow screws on the top head of the blasthead, as shown in Fig. 8. The manufacturing process is as follows: 1) to make the head of this blasthead, as shown in Fig. 2; 2) to make the other parts, vacuum pipe, blasting rectangular duct, and to drill three even holes on the surface of the head of the blasthead; 3) to weld the three parts together.

Blasting sensors

Two types of blasthead sensor system, a radiological characterization sensor system and a lift-off sensor system, are proposed to be incorporated with the blasthead for reducing operator dependency. The entire blasthead configuration is depicted in Fig. 9, with three "lift-off" sensors shown beside the blasthead and two radiological sensors fixed adjoining the blasting nozzle and blasting vacuum, respectively.

For radiological characterization sensor system, there are four major subsystems: transducers (2); transducer interface electronic modules (2); control electronic module; and operator interface module. The transducers (2) were incorporated into the structure of the blasthead as compactly as possible to minimize the standoff distance from an adjacent perpendicular surface, as shown in Fig. 9. A transducer is situated in the forward path, and a second transducer is situated in the following path of the blasthead. This arrangement allows feedback to the operator indicating degree of contamination and success at decontamination.

For the lift-off sensor system, there are three capacitive proximity sensors fixed around the blasthead face. This sensor system will be used with a pinch-off valve to cut the flow to the blasthead when a lift-off condition occurs. Also, it can prevent ineffective cleaning while the blasthead is in lift-off condition. Figure 10 shows the system block diagram of this lift-off sensor system.

The lift-off detection logic determines if any of the three proximity sensors doesn't detect the surface below. If it doesn't, it triggers the time delay to start waiting. At the end of the time delay, the relay will lose power and the blasting will stop. The time delay will be used to avoid false triggers and to keep the blasthead from triggering off and on multiple times a second. The lift-off

system is designed so that the blasthead will not operate without power or with one or more of the sensors disconnected.

Dust Separators

Based on model test results, the major dimensions of the centrifugal separator have been optimized, especially for reducing the height of the separator. The revised centrifugal separator equals the previous separation efficiency and will be more stable. The modified centrifugal separator is shown in Fig. 11.

Since the nozzle shape changed from a round to a rectangular channel, the nozzle's cross-section became a narrow and long rectangular channel. Because of this, the channel is easily blocked when the system is operational, especially when clearing concrete wall surfaces. Therefore, the new vibration pre-separator for larger particles with low density was designed and fabricated. The principal of this pre-separator is a plastic tube with a sieve held in vertical position. A hammer is employed to hit the plastic tube frequently to disengage the large particles blocked by the sieve. The large particles will drop into the collection box. The new separator is easy to fix and remove from the operating system to accommodate different working conditions and purposes.

The test results showed that the pre-separator could work well for separating the large-size particles. Waste with some large-size particles was fed to the two separators for evaluating their efficiency. The sieve with 2mm mesh chosen from three mesh sizes was used in the pre-separator. The pre-separator can successfully separate the large and low-density particles from the fine abrasive and dust on cleaning the concrete wall. Under this test condition, the pre-separator can continue to work for more than five hours. Then the sieve in the pre-separator should be cleaned because some particles with sizes almost the same as the mesh size can choke it.

Pre-prototype testing

The pre-prototype unit testing was performed for cleaning the coated steel plate and concrete wall by using the redesigned vacuum blasting system and the baseline technology. Table 3 lists the test cases.

Table 3.
Test surface and removal media description

ID No.	Removal Media Used	Demonstrated Surface Media	Size of Area Assigned	Test Surface Media Description	Demonstrated Geometry
1 (New)	80-grit	Carbon Steel	4 ft^2	Coated metal plate with an epoxy polyamine coating primer of 8 mils Ply-Mastic and 8 mils Ply-Thane 890 HS. 4x4x¼" thick	Plate
2 (New)	80-grit	Concrete Wall	4 ft^2	Concrete-poured, with an epoxy polyamine coating primer of 7 mils Ply-Mastic and 1.5 mils Ply-Thane 890 HS. The coated concrete ceiling has the dimension of 4x4 with a compression strength between 4420 to 5660 psi.	Plate
3 (Baseline)	40-grit	Carbon Steel	4 ft^2	Coated metal plate with an epoxy polyamine coating primer of 8 mils Ply-Mastic and 8 mils Ply-Thane 890 HS. 4x4x¼" thick	Plate
4 (Baseline)	40-grit	Concrete Wall	4 ft^2	Concrete-poured, with an epoxy polyamine coating primer of 7 mils Ply-Mastic and 1.5 mils Ply-Thane 890 HS. The coated concrete ceiling has the dimension of 4x4 with a compression strength between 4420 to 5660 psi.	Plate

The test results for production rate and comparisons are listed in Table 4.

Table 4.
Test results

	Production Rate (ft^2/hr) Coated Steel Plate	Production Rate (ft^2/hr) Concrete Wall
Redesigned System (NEW)	13.3 (ID no.1)	33.2 (ID no.2)
Baseline Technology	9.8 (ID no.3)	21.8 (ID no.4)
Increase of Redesigned System to Baseline Technology	36%	52%

As shown in Table 4, for the coated steel plate, the productivity rate of the redesigned system was increased by 36%. And for the concrete wall, the productivity rate of the redesigned system was increased by 52%. The main reasons affecting the productivity rate of the pre-prototype are 1) the new blasthead is heavy and cumbersome and not user-friendly because it is designed as a testing model; 2) the operator finds it ergonomically hard to handle the new blasthead due to its heavy weight. The test results indicate that the redesigned system works well and almost meets the

design goal. Of course, further modification will be needed to improve the performance of the redesigned system.

The pre-prototype design is for research and lab testing, not for commercial use. The weight of the new blasthead is 3 lb more than the LTC baseline one. With a reduction of the blasthead weight and a more user-friendly configuration, the performance of the new blasthead can be expected to increase productivity by at least a further 10% in the Phase III final design.

CONCLUSION

1. Numerical simulation can be used to study the two-dimensional flow in certain components of the vacuum blasting system, as well as the whole system. The numerical predications are reasonable and can be used to determine the optimal parameters in the practical design processes. Comparing the velocity distribution and separation efficiency of the experiment to the numerical modeling shows that the experimental results and the estimated data agree fairly well and with a deviation within ±10%.
2. New materials, tungsten carbide, boron carbide, and Roctec 500, were selected to manufacture the liner to the rectangular blasting nozzle for testing their lifetime. All materials were good for fabrication of the nozzle liner, but the boron carbide being much lighter is the preferred one.
3. Two separators, the pre-separator designed for large low-density particles created by cleaning the concrete wall and the centrifugal separator designed for separating the fine grits from the dust, have been designed and fabricated, and their separation efficiencies have been measured. The test results show that the two separators can work well as expected. The separation efficiency of the centrifugal separator for the G80 grits was almost double that of the old one.
4. The radiological sensors and their electronic control system were tested by using the simulated radiation source in the lab. The result indicated the design of the rad sensor and its electronic control system was successful. The rad sensor can efficiently detect the level of contamination on the surfaces.
5. The “lift-off” sensor system consisted of three proximity sensors and the electronic control system. It was designed to incorporate with the blasthead. Both the lab test and on-site test indicated this system can shut off the trigger successfully when the blasthead is taken from the surface, as expected.
6. The pre-prototype unit testing has been performed at FIU-HCET’s site. The whole redesigned vacuum blasting system works successfully for cleaning the different media surfaces. The productivity rate and the economy of the redesigned system were increased almost 50% over the baseline technology.
7. The information about how to further improve the performance of the redesigned vacuum blasting system has been gathered. The following issues need to be considered in the final design of the prototype and will be finished in Phase III:
   - Minimize the blasting head size and weight.
   - Change the blasting nozzle angle to a more vertical position.
   - Reduce the size of the pre-separator.

- Improve the "lift-off" sensor by using an automatic valve control system and move the valve as close to the blasthead as possible.

ACKNOWLEDGMENT

Support for this work was provided by the Department of Energy (DOE) under Contract No. DE-AR26-98FT40367. The authors gratefully acknowledge the efforts of Lee Schneider, Walter Conklin, David Guasca, Amer Awad, and Leonel Lagos at FIU-HCET for their valued work in this project.

REFERENCES

Baliga, B.R., and Patankar, S.V., 1983, "A Control Volume Finite-Element Method for Two-Dimensional Fluid and Heat Transfer," Numerical Heat Transfer 6, 245–261.

FLUENT Inc., 1999, FLUENT 5 User Guide.

Launder, B.E., and Spalding, D.B., 1972, Lectures in mathematical models of turbulent flows, Academic Press, London, England.

McPhee, W.S. and van Leeuwen, J., 1988, A New Type of Vacuum Blasting Equipment for Removing Lead-based Paints, Proceedings of the SSPC Symposium Removing Lead Paints From Steel Structures and the FHWA Workshops on Bridge Paint Removal, February 28 –March 3, 1988, Washington, D.C.

McPhee, W.S., and Waagbo, S., 1992, Evaluation of abrasive recycling characteristics of several abrasives in vacuum blasting, Proceedings of the SSPC's 5th Annual Conference on Industrial Lead Paint Abatement and Removal, 1992.

McPhee, W.S., and Ebadian, M.A., 1999, High productivity vacuum blasting system, Proceeding of DOE Conference for Industry Partnerships to Deploy Environmental Technology, October 12-14, 1999, Morgantown, WV.

McPhee, W.S., Lin, C.X., Zheng, B., Kang, H.J., Welker, K., Ade, R., and Ebadian, M.A., High Productivity Vacuum Blasting System, Proceeding of the U.S. Department of Energy's 4th International Decommissioning Symposium, June 12-16, 2000, Knoxville, TN.

Morsi, S.A., and Alexander, A.J., 1972, An investigation of particle trajectories in two-phase flow systems, Journal of Fluid Mechanics, 55(2), 193-208.

Seavey, M., 1985, Abrasive Blasting above 100 psi, Journal of Protective Coating & Linings, 26-37, July 1985.

Settles, G.S., and Garg, S., 1994, A scientific view of the productivity of abrasive blasting nozzles, Proceedings of the SSPC's Managing Costs and Risks for Effective and Durable Protection Seminars, November 11-17, 1994, Atlanta, Georgia.

Settles, G.S., and Gepprt, S.T., 1996, Redesigning blasting nozzles to improve productivity, Journal of Protective Coating & Linings, 64-72 October 1996.

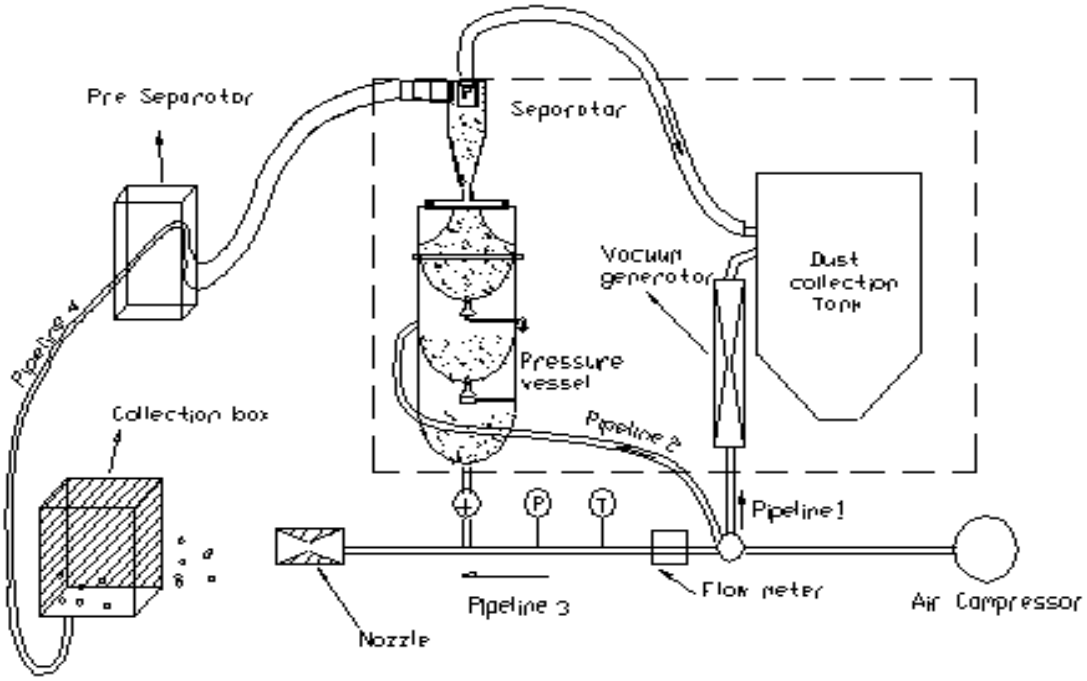

Fig. 1 Experimental setup of flow velocity in nozzle and separator and separation efficiency measurement.

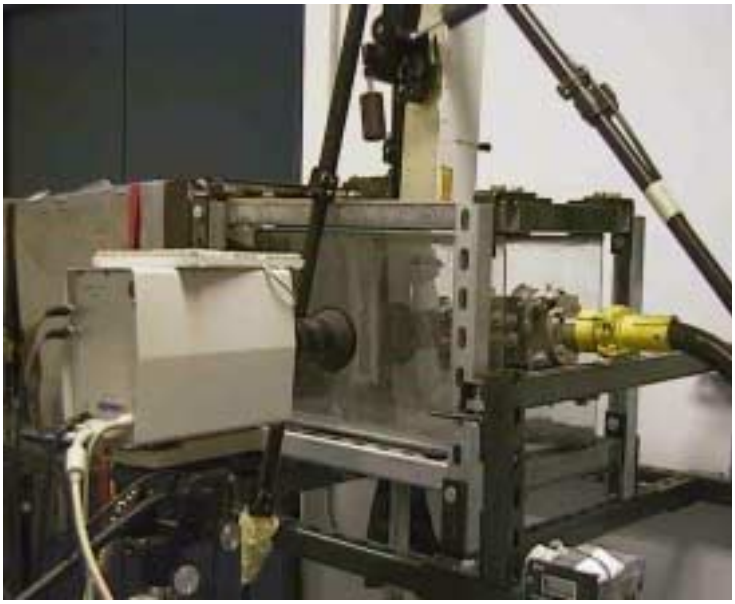

Fig. 2 The test section for measuring blasting nozzle velocity and construction.

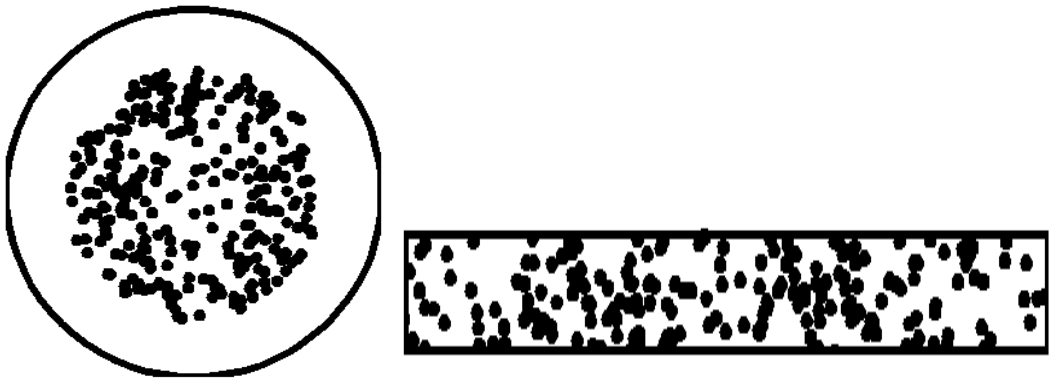

Fig. 3 Particle distribution at exit plane of the nozzles (left: round nozzle; right: rectangular nozzle).

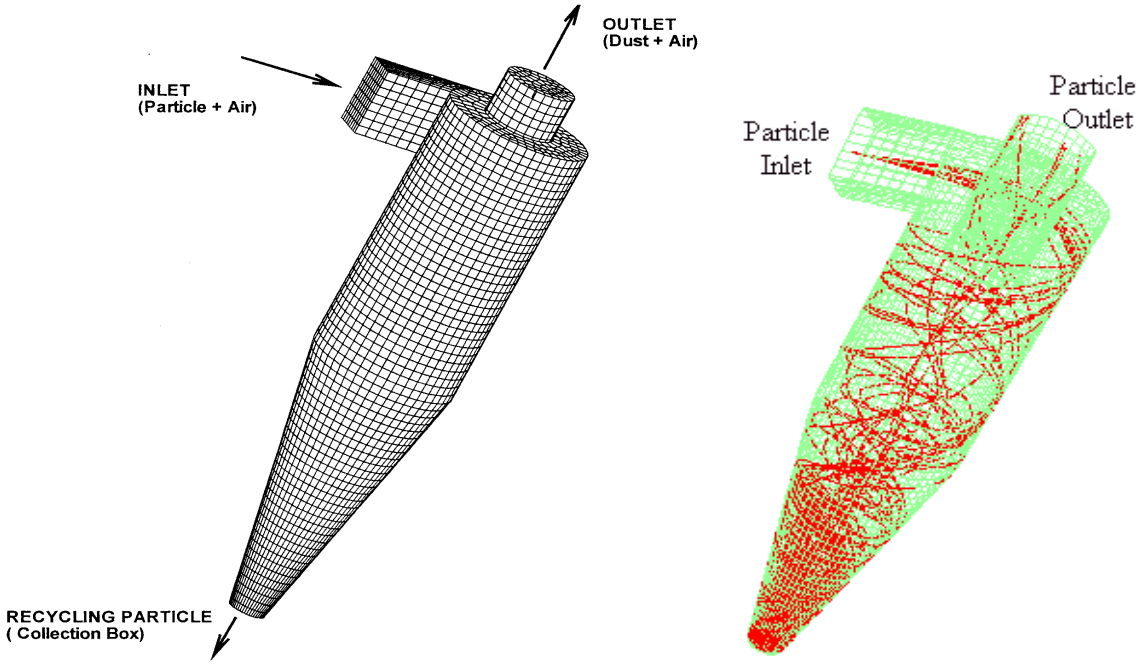

Fig. 4 The schematic grid system (left) and particle trajectories (right) in the centrifugal separator.

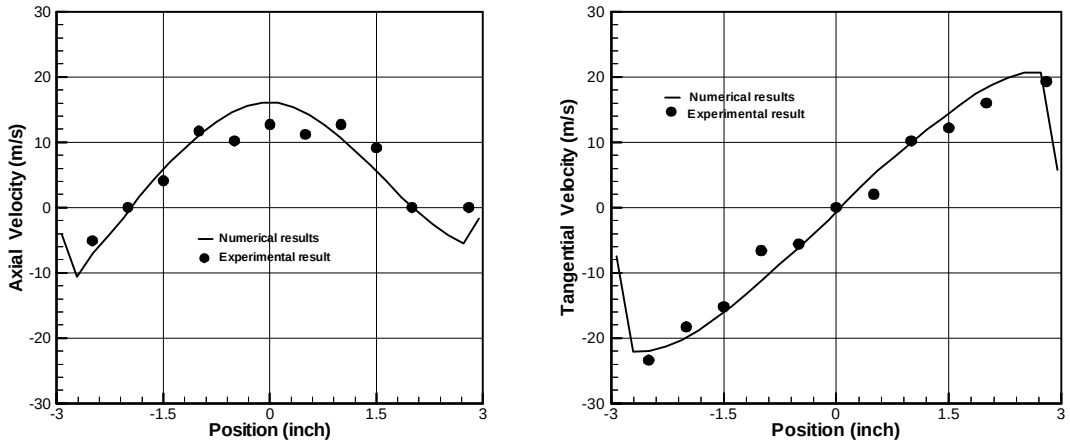

Fig. 5 Comparison of numerical results and experiment data in the axial (left) and tangential (right) direction at the lower position (i.e., 152.4 mm (6 inches) to the separator's top surface).

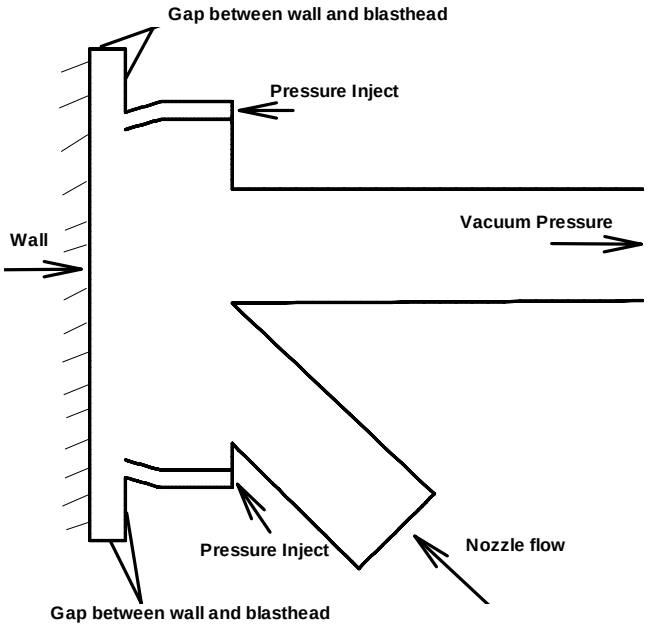

Fig. 6 Proposed geometry of the wind curtain.

Fig. 7 New rectangular nozzle (half piece).

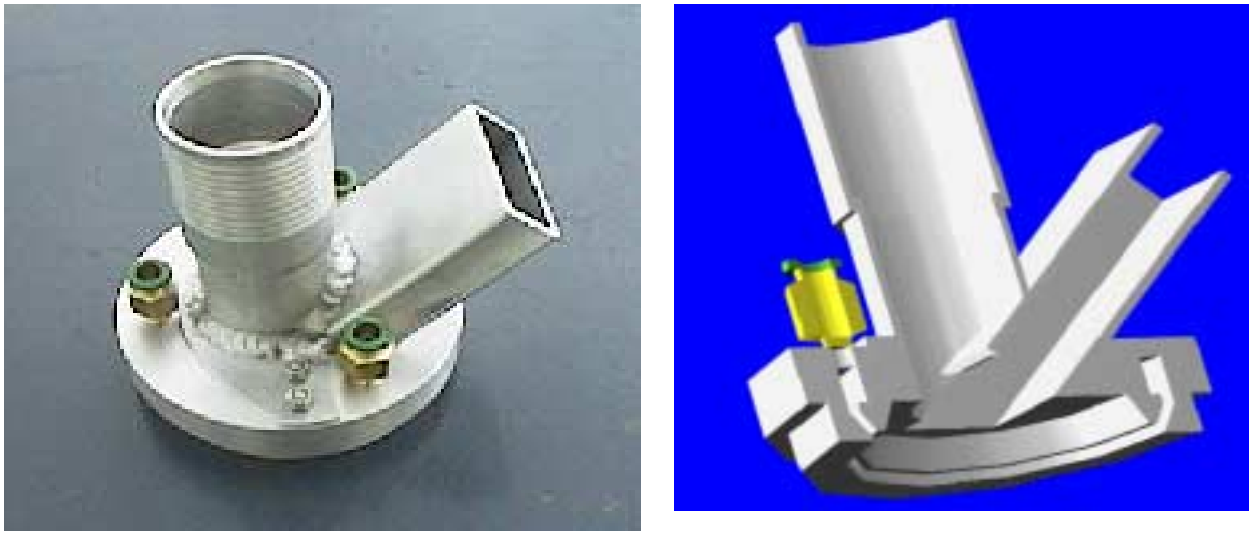

Fig. 8 New blasthead design (right: section view).

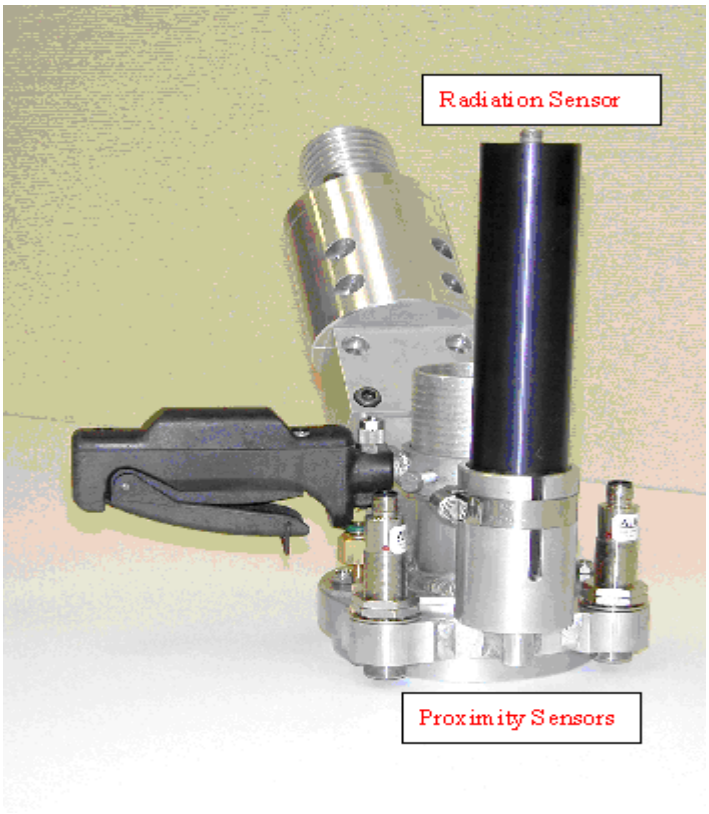

Fig. 9 New blasthead design with addition of radiological and proximity sensors.

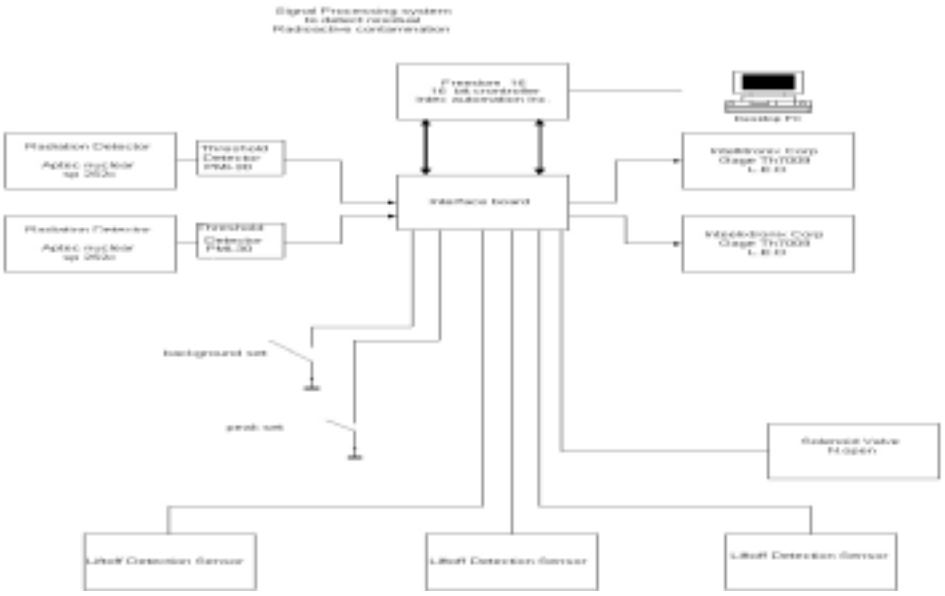

Fig. 10 System block diagram.

Fig. 11 New centrifugal separator.